Supporting information

Defect-Suppressed Titanium Oxynitrides via Topochemical Nitridation using Ca_3N_2

Yuki Sasahara,[+] Kento Yoshii,[+] Daichi Kato, Issei Yamamoto, Yusuke Tsutsui, Kei Morisato, Hikaru Takeuchi, Tatsuya Tsumori, Hiroshi Takatsu, Satoshi Horike, Shu Seki, Kazuhiko Maeda, and Hiroshi Kageyama*

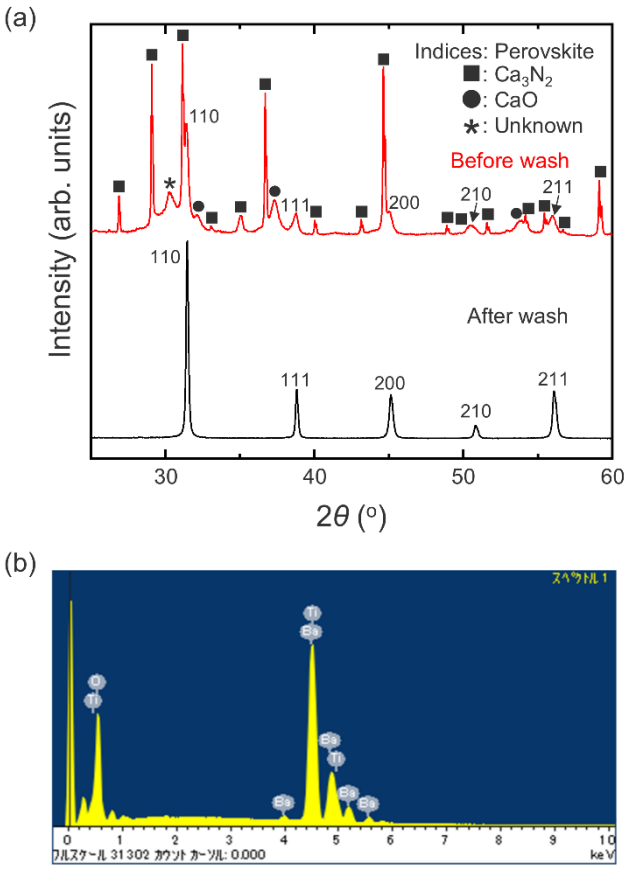

Figure S1. (a) Powder XRD patterns of $BaTiO_{3-3x/2}N_x$ samples (~100 nm) reacted with Ca_3N_2 at 550 °C for 2 weeks, before (red) and after washing (black). Extra peaks due to residual Ca_3N_2, CaO, and minor unknown phases disappear after washing, leaving only the perovskite reflections. (b) Elemental analysis of the washed sample using SEM-EDS. No Ca peak (~3.69 keV) was detected. The peak C is attributed to the carbon tape used to fix the powder.

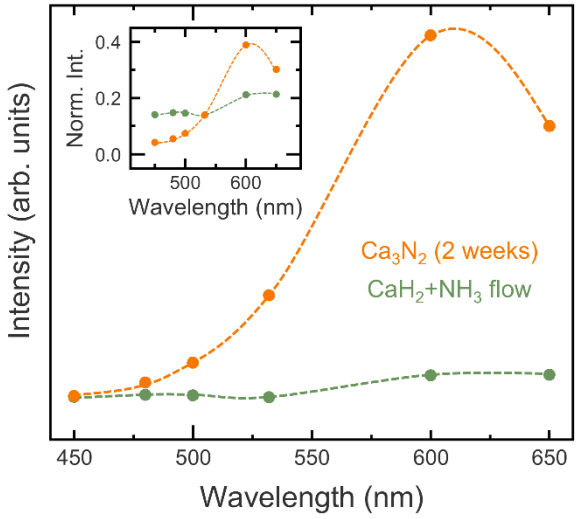

Figure S2. PL spectra of $BaTiO_{3-3x/2}N_x$ measured at 6 K. The Ca_3N_2-treated sample (orange) exhibits a strong band-edge emission (~2.0 eV, 600 nm) with no discernible mid-gap emission, whereas the ammonolysis-derived sample (green) shows weak and broadened emission consistent with defect-induced nonradiative recombination. The inset shows normalized spectra highlighting the difference in spectral shape. Dashed lines are guides to the eye.

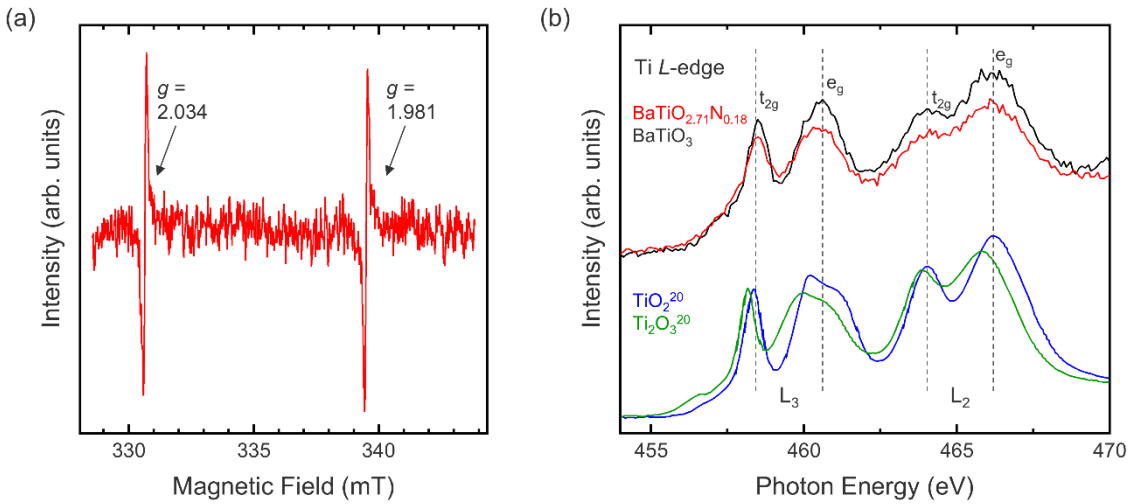

Figure S3. Spectroscopic assessment of the Ti valence state. (a) Electron paramagnetic resonance (EPR) spectrum of Ca_3N_2-derived $BaTiO_{3-3x/2}N_x$ measured at room temperature. The sharp signals at g = 2.034 and 1.981 arise from Mn^{2+} in the MgO (Mn/MgO) standard used for magnetic field calibration. No discernible signal attributable to Ti^{3+} was observed within the experimental sensitivity. (b) Ti *L*-edge soft X-ray absorption spectroscopy (XAS) spectra of the same specimen measured in partial fluorescence yield (PFY) mode, together with precursor $BaTiO_3$ and reference compounds TiO_2 (Ti^{4+}) and Ti_2O_3 (Ti^{3+}). The spectra of TiO_2 and Ti_2O_3 were taken from Ref. 20. The peak positions of $BaTiO_{3-3x/2}N_x$ closely overlap with those of $BaTiO_3$ and TiO_2, with no resolvable contribution from Ti^{3+} detected within the detection limit.

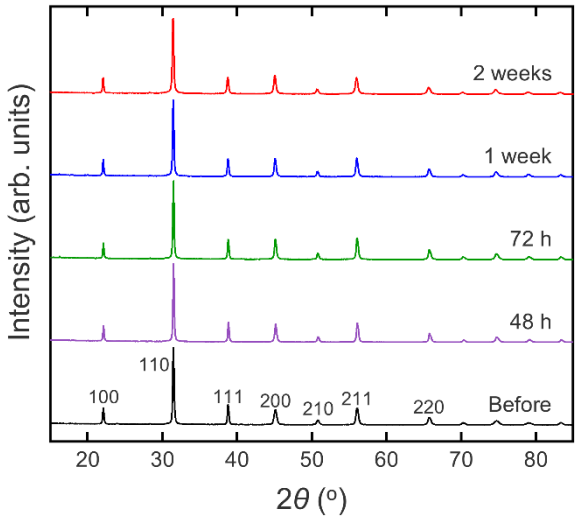

Figure S4. Powder XRD patterns of $BaTiO_{3-3x/2}N_x$ samples (~100 nm) reacted with Ca_3N_2 for different durations, followed by washing to remove residual Ca_3N_2 and the CaO byproduct.

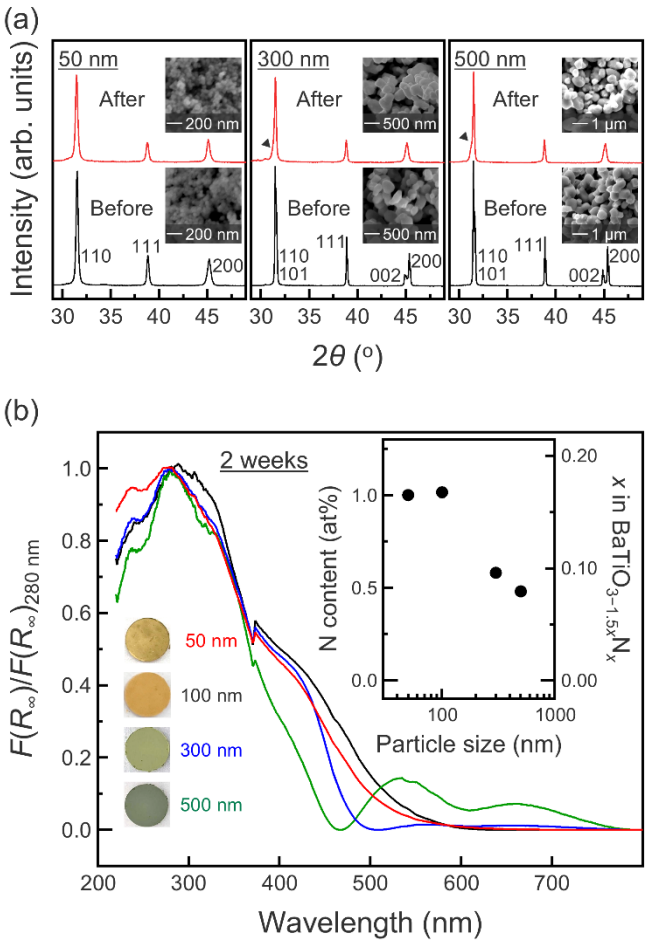

Figure S5. (a) Powder XRD patterns of $BaTiO_{3-3x/2}N_x$ prepared from $BaTiO_3$ precursors with different particle sizes (~50, 300, 500 nm) after the reaction with Ca_3N_2 for 2 weeks. The indexed reflections correspond to $BaTiO_{3-3x/2}N_x$ (space group: *Pm*−3*m* for 50 nm, *P*4*mm* for 300 and 500 nm). The insets are SEM images of the respective samples. (b) Normalized UV-vis diffuse reflectance spectra of $BaTiO_{3-3x/2}N_x$ reacted with Ca_3N_2 for 2 weeks, as a function of the precursor particle size of precursor $BaTiO_3$. Insets (left) show photographs of the samples. Insets (right) summarize the nitrogen content as a function of precursor particle size.

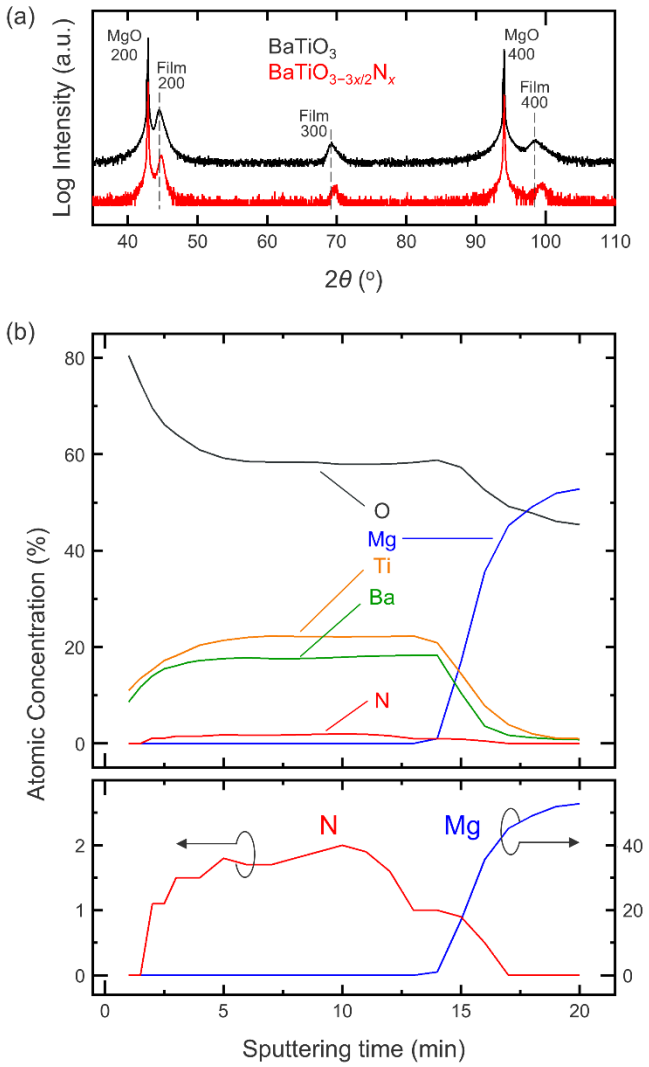

Figure S6. (a) Out-of-plane XRD patterns of $BaTiO_3$/MgO(100) thin films as-deposited and after Ca_3N_2 nitridation at 550 °C for 2 weeks. (b) XPS depth profiles of Ba, Ti, O, N, and Mg for the nitrided film shown in (a), obtained by sequential Ar^+ sputtering. The nitrogen signal is observed throughout the film thickness and decreases at the film/substrate interface, identified by the rise of the Mg signal from the MgO substrate.

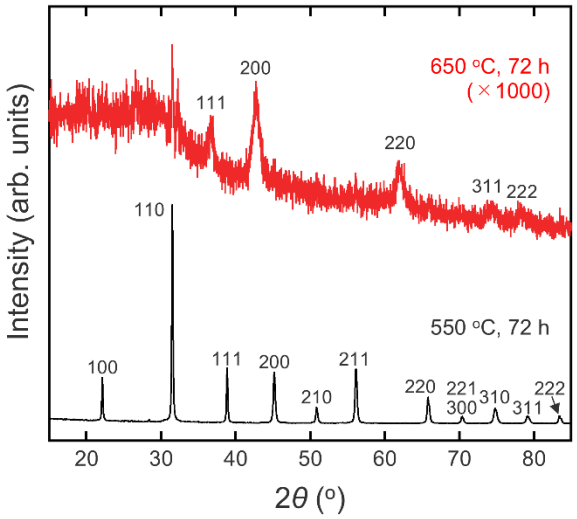

Figure S7. Powder XRD patterns of $BaTiO_{3-3x/2}N_x$ samples (~100 nm) reacted with Ca_3N_2 at 550 °C and 650 °C for 72 h, followed by washing to remove residual Ca_3N_2 and the CaO byproduct. At 550 °C, sharp reflections are indexed to the perovskite phase ($BaTiO_{3-3x/2}N_x$), whereas heating at 650 °C leads to further reaction, producing TiN, accompanied by broad, amorphous-like features.

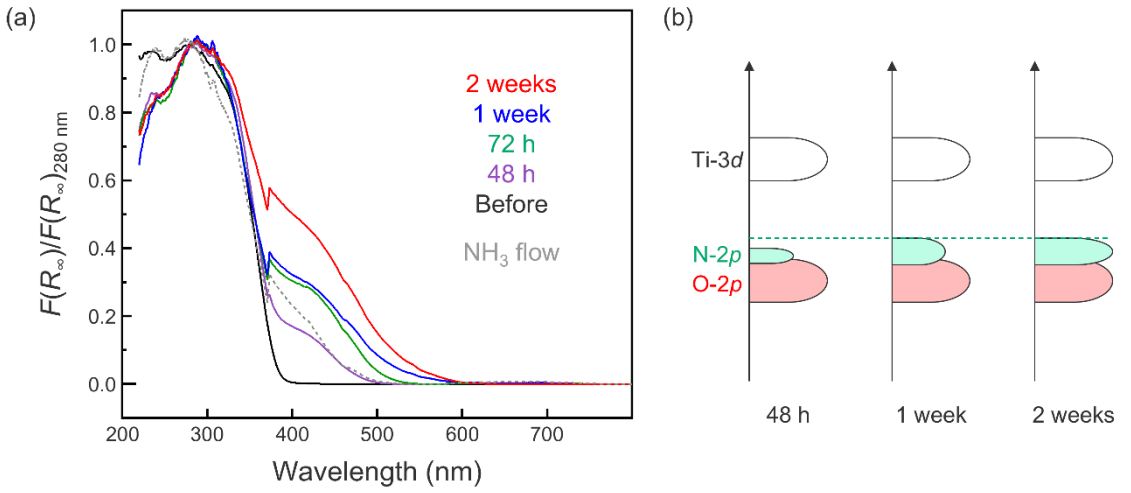

Figure S8. (a) Normalized UV-vis diffuse reflectance spectra of $BaTiO_{3-3x/2}N_x$ (~100 nm) as a function of reaction time with Ca_3N_2, demonstrating progressive enhancement of visible-light absorption with prolonged reaction time. (b) Schematic illustration summarizing the evolution in the UV–vis absorption spectra shown in (a), based on the corresponding changes in the electronic structure near the band edge.

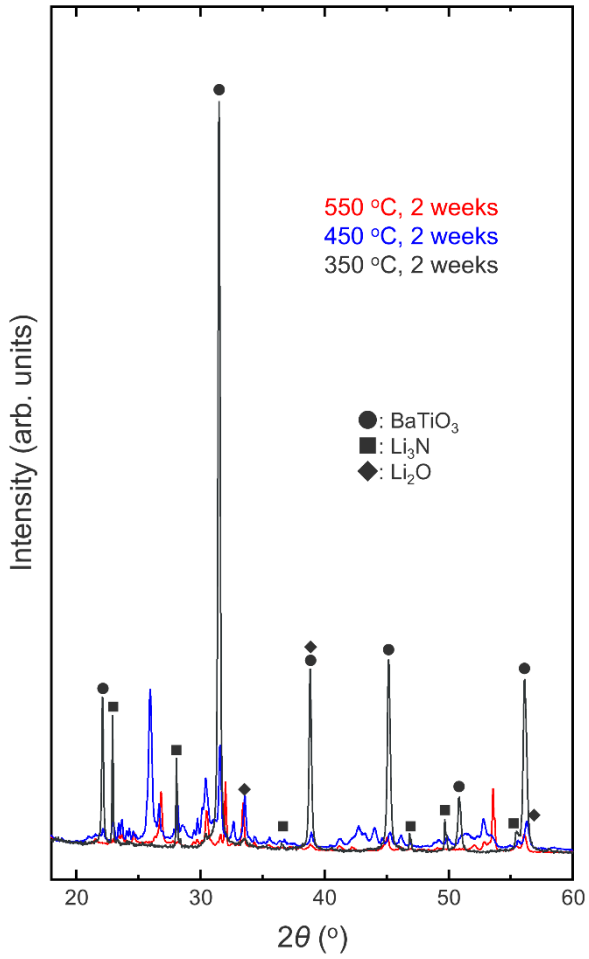

Figure S9. Powder XRD patterns of products obtained by reacting $BaTiO_3$ nanoparticles (~100 nm) with Li_3N at 350, 450, and 550 °C for 2 weeks. The products were measured without washing. Upon treatment at ≥ 450 °C, a pronounced decrease in the intensity of $BaTiO_3$ reflections, indicating progressive decomposition of the perovskite phase. A similar trend is observed for the sample treated with Ca_3N_2 at 650 °C (Fig. S7).

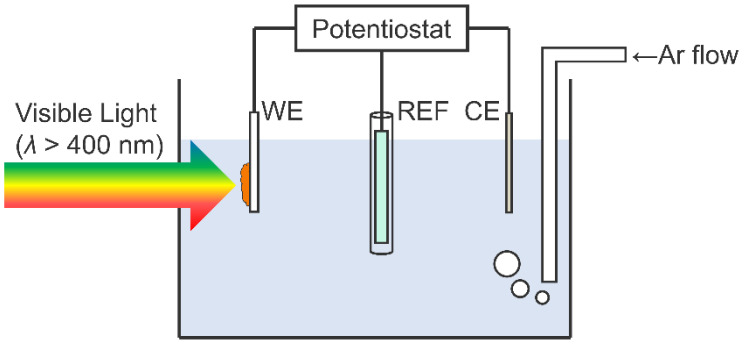

Figure S10. Schematic illustration of the three-electrode photoelectrochemical setup. A working electrode (WE), reference electrode (REF; Ag/AgCl), and counter electrode (CE; Pt wire) were connected to a potentiostat. Visible light (λ > 400 nm) was irradiated onto the working electrode, and the electrolyte was deoxygenated by Ar flow.

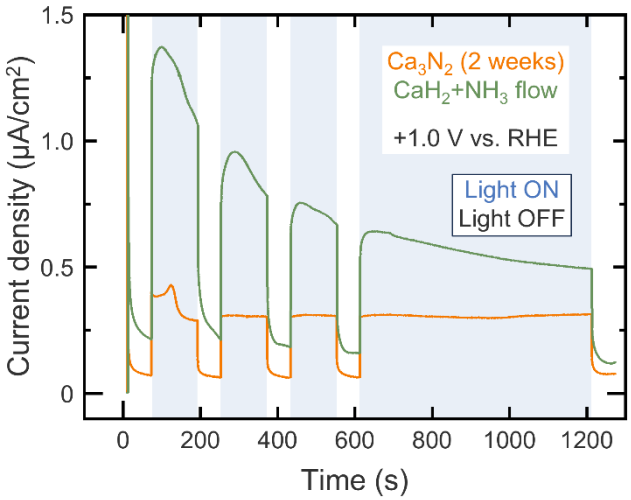

Figure S11. Transient photocurrent responses of $BaTiO_{3-3x/2}N_x$/FTO electrodes at +1.0 V vs. RHE in 0.1 M Na_2SO_4 solution under visible-light irradiation (λ > 400 nm). The oxyhydride-derived sample (green) shows a higher initial photocurrent but rapidly degrades under illumination due to defect-mediated self-oxidation, whereas the Ca_3N_2-treated sample (orange) exhibits a smaller but stable photocurrent.

Table S1. Lattice constant (a), nitrogen content, and optical bandgap of $BaTiO_{3-3x/2}N_x$ (~100 nm) as a function of reaction time with Ca_3N_2 at 550 °C. These values were used to generate the plots in Fig. 2a. For reaction times up to 168 h, uncertainties in a represent the standard uncertainties obtained from Le Bail analysis of laboratory XRD data. For 2 weeks, a is reported as the mean value with standard deviation derived from 14 independently prepared samples, and the nitrogen content as the mean value with standard deviation from 4 independently prepared samples. Bandgaps were estimated from Tauc analyses of diffuse-reflectance spectra. In some cases, two indirect absorption edges (lower- and higher-energy transitions) are observed and both values are listed.

Reaction time (h)	a (Å)	N content (at%)	x in $BaTiO_{3-3x/2}N_x$	Bandgap (eV)
0	4.01433(6)	0	0	3.14
6	4.01037(7)	-	-	-
12	4.01001(7)	-	-	-
24	4.01080(7)	0.11	0.02	-
48	4.01098(5)	0.10	0.02	2.40 / 3.00
72	4.01327(5)	0.49	0.08	2.30 / 2.82
168 (1 week)	4.01557(5)	0.70	0.12	2.07 / 2.73
336 (2 weeks)	4.0191(9)	1.03(12)	0.17(2)	2.03 / 2.26

Table S2. Melting points[18,27] of nitridation reagents and resulting lattice constants of $BaTiO_{3-3x/2}N_x$ after reaction at 550 °C for 2 weeks. The lattice constant of $BaTiO_3$ heated under the same conditions is also shown as a control. For the sample reacted with Ca_3N_2, *a* is reported as the mean value with standard deviation from 14 independently prepared samples.

Compounds	Melting point (°C)	Lattice constant (Å)
Ca_3N_2	1195	4.0191(9)
VN	2050	4.00902(8)
ZrN	2952	4.01029(15)
None	-	4.00803(11)